Supplementary Material: The Sub-band Structure of Atomically Sharp Dopant Profiles in Silicon

Federico Mazzola,[1,2] Chin-Yi Chen,[3] Rajib Rahman,[3,4] Xie-Gang Zhu,[5]
Craig M. Polley,[6] Thiagarajan Balasubramanian,[6] Phil D. C. King,[2]
Philip Hofmann,[7] Jill A. Miwa,[7] and Justin W. Wells[1,*]

[1]*Center for Quantum Spintronics, Department of Physics, Norwegian University of Science and Technology, NO-7491 Trondheim, Norway*

[2]*SUPA, School of Physics and Astronomy, University of St Andrews, St Andrews, Fife KY16 9SS, UK.*

[3]*Department of Electrical and Computer Engineering, Purdue University, West Lafayette, IN 47907, USA*

[4]*School of Physics, The University of New South Wales, Sydney, New South Wales 2052, Australia*

[5]*Science and Technology on Surface Physics and Chemistry Laboratory, Mianyang 621908, China*

[6]*MAX IV Laboratory, PO Box 118, S-22100 Lund, Sweden*

[7]*Department of Physics and Astronomy, Interdisciplinary Nanoscience Center (iNANO), University of Aarhus, 8000 Aarhus C, Denmark*

(Dated: April 27, 2020)

METHODS

Sample preparation

'Standard' single-dose Si:P δ-layers (i.e. as used in all figures except Fig. 2(b) and (c)) are prepared using a PH_3 dose performed at $\approx 5 \times 10^{-9}$ mbar (from a base pressure of $\approx 1 \times 10^{-10}$ mbar) for 5 minutes, yielding P concentrations similar to that reported in Ref. 1, i.e. slightly less than 25% of a monolayer (ML). 'Double dose' samples (i.e. as used in Fig. 2(b)) are prepared using the same procedure, but with the inclusion of an additional annealing cycle to incorporate dopants into the surface, followed by a second PH_3 dose. This approach gives a higher degree of dopant disorder and a higher dopant density ($> 25\%$) as described in Ref. 2. 'Thick' samples (as used in Fig. 2(c)) are prepared by depositing Si in a high background pressure (1×10^{-6} mbar) of PH_3 , yielding a similar dopant density (i.e. $\approx$ 25%) but a larger total number of dopants, in a disordered and significantly thicker dopant plane (≈ 1.5 nm in this case, c.f. < 0.5 nm for standard single-dosing). After forming the dopant plane, ≈ 2 nm of epitaxial silicon encapsulation is grown on top, and the sample is flash annealed to 500°C to improve the crystal quality and remove excess hydrogen from the surface.

So-called 'dummy' samples were also created (see for example Fig. 1(e) in the main document). In this case, the growth is carried out similarly to the 'standard' single dose sample described above, except that the step in which PH_3 would be introduced has been skipped. i.e. this sample comprises a clean Si substrate with an Si epitaxial overlayer, but *without* the δ-layer of dopants. In all other aspects (i.e. growth, cleaning, annealing), the sample is similar to the δ-layer samples. The purpose of this 'dummy' is to demonstrate that the reported 1Γ, 2Γ and 3Γ electronic states must be due to the dopant plane (and not an artefact of some other aspect of the sample growth). Further studies of simialr 'dummy' samples can be found in Ref. 1.

Tight Binding calculations

The Si:P δ-doped layer's band structure is modelled by an empirical $sp^3d^5s^*$ tight binding (TB) model coupled with the Poisson equation [3]. The phosphorus donor is explicitly assigned in the simulation domain as a truncated Coulomb potential. The parameter is

benchmarked with a single electron ground state energy level (45.6 meV) [4, 5]. In the self-consistent charge-potential Schrödinger-Poisson calculation, the electron-electron interaction is taken into account through local density approximation. The electron screening is determined by the dielectric constant (ε) in the Poisson equation.

We also point out that the role of the dielectric constant in the Slater-Koster tight-binding (TB) theory is not the same as in *ab-initio* density functional theory (DFT). In DFT, typically the core and the valence electrons are considered, and the electronic density is computed by populating all these electronic states up to the Fermi level through self-consistent iteration of the Kohn Sham equations. Hence, a dielectric constant of vacuum can be used, and the effective dielectric constant can be extracted from the method.

In contrast, in the semi-empirical Slater-Koster TB method used here, the atomic basis functions responsible for valence bonding only are optimized to reproduce the bulk band-structure of the material without performing any self-consistent iterations of the charge density in the process. Hence, the Slater-Koster TB method in its original form cannot reproduce the dielectric constant of the material.

In our case, we are considering the charge self-consistency of the donor electrons only (i.e. the extra bound electron which does not participate in bonding with Si atoms, while assuming the background Si bonds remain frozen). Hence, we have to solve the Poisson equation with the dielectric constant of the material environment. This is a standard technique in atomistic device simulations where the Poisson and Schrodinger/Green's functions are solved self-consistently with the material dielectric constant as an input [6–8].

ASYMMETRIC POTENTIAL

It is conceivable that symmetry breaking in one form or another could give rise to additional bands in the bandstructure; we therefore consider this possibility. Ideally, when making a δ-layer sample, one aims to create a confinement potential which is symmetric in the cross-section. However, it is clear that this is generally not achievable. Specifically, atom probe tomography and secondary ion mass spectrometry measurements show a tendency for the dopants to segregate more towards the surface side than into the bulk of these systems [9]. In addition, the Fermi level pinning at the surface may be different from in the bulk [1] because of surface contamination, dopant segregation, the presence of partially filled surface

states, etc; thus an asymmetric potential is fully expected. On the other hand, to the best of our knowledge, all published calculations work on the assumption that the confinement potential is symmetric above and below the dopant plane.

Asymmetry in the doping potential can be readily incorporated in the TB calculations, thus allowing the effects of such an asymmetry in the band structure to be studied. To describe the segregation of the P atoms, it is reasonable to assume that P atoms are also present in a layer adjacent to the main P plane: we therefore built a doping profile modelled on the configuration shown in Supplementary Figure 1(b), where the main P plane (0.25 ML of P atoms) is followed by a less doped layer (here, we have chosen to use 1/8 or 0.125 ML of P atoms to approximate the segregation). This is a realistic approximation, albeit very simple, and hence the TB model should be able to capture the effects caused by this asymmetry. In order to facilitate a comparison, we have repeated the TB calculations using this commonly accepted assumption of a symmetric doping profile (Supplementary Figure 1(a)).

The effect of an asymmetric doping profile can be summarized as follows: (i) the valley-splitting is slightly reduced, and (ii) no new occupied bands are expected. The next unoccupied band with a parabolic minimum (labelled 3Γ) is calculated to be so far above the Fermi level that it is unfeasible to consider that it may be seen in the measured data.

It is worth pointing out that we have also created a number of other arbitrarily asymmetric doping profiles, and the trend in the TB calculated bandstructure remains the same: the valley splitting tends to reduce, but no additional bands near the Fermi level are expected. Thus we infer that this asymmetry cannot explain the experimental observation of an additional band.

SPIN-ORBIT COUPLING

Whilst the invariance of the measured bandstructure with respect to the sample preparation already leads us to believe that the in-plane ordering of the dopants is not responsible for the additional band in the bandstructure, it is worth considering possible symmetry breaking more rigorously. For example, it is conceivable that the high density ($\approx 25\%$) of dopants form a structure which breaks the in-plane inversion symmetry. Such symmetry breaking can give rise to bands which are non-degenerate with respect to their spin [10, 11], which could potentially lead to 1Γ having two branches. Furthermore, the splitting would

be expected to be zero at $k_{\|} = 0$, and would not necessarily be isotropic in $k_{\|}$. Thus qualitatively, it is possible to imagine that spin-orbit coupling (SOC) could give rise to a splitting in the bandstructure which scales approximately as $\propto Z^4$, and hence is expected to be weak (but not necessarily negligible [12, 13]) in Si:P.

A quantitative estimate of the expected SOC strength in Si:P δ-layers has been obtained by relativistic TB calculations, confirming the small role played by this effect in such a light system. This is shown in Supplementary Figure 1(c) where the values of the SOC strength in the k_x and k_y directions (green line) and the k_{xy} direction (blue line) are shown. The TB calculations include Rashba, Dresselhaus and higher order k-terms, nevertheless the maximum strength of the SOC obtained is less than 0.8 meV, a value approximately 40$\times$ smaller than our experimental energy resolution, and about 120$\times$ smaller than the energy separation of the experimentally observed energy separation at the Fermi level crossing in k_y.

Although the relativistic TB already indicates that the SOC is very small, surprising reports of unusually strong SOC in very light elements, such as diamond, also exist [14]. In order to further illustrate how this *cannot* be the origin of the observed splitting in the Si:P bandstructure, we therefore carried out an additional estimate in which the SOC strength is artificially 'forced' to match the observed electronic structure: We assume *ad absurdum* that SOC is the reason behind the observed band splitting. In such a case, the splitting observed in the ARPES measurements of Fig. 2 cannot occur via the Rashba-Bychkov effect for which isotropic spin-split Fermi surfaces are expected [15]: At the Fermi level, in Fig. 2, the Fermi surfaces collected for different Si:P δ-layers show a strong dependence of the splitting on the momentum direction, i.e. the splitting is maximum along k_x and k_y and minimum (possibly zero) along k_{xy}. Therefore, if SOC is responsible for the existence of the sub-band structure via spin-degeneracy removal, it has to be due to higher order k-terms, for example $\propto k^3$, since the higher order terms are not necessarily isotropic. Such higher order SOC is common in binary semiconductors such as GaAs, where the spin-degeneracy is lifted resulting in $E_{1,2}(k) = E_0(k) \pm \Delta E(k)$, where,

$$\Delta E(k) = \gamma/2[k^2(k_x^2k_y^2 + k_y^2k_z^2 + k_z^2k_x^2) - 9k_x^2k_y^2k_z^2]^{\frac{1}{2}} \quad (1)$$

with γ describing the strength of the coupling as in Ref. 16. If we adopt this model to 'dress' a simple parabolic dispersion to describe the electronic structure of Si:P δ-layers we obtain an

excellent agreement with the experimental data as demonstrated in Supplementary Figure 1(d,e). However, in order to obtain such an agreement we had to force the parameter γ, to be $\gamma = 305$ eVÅ^3. This value is approximately 18 times larger than the value describing the SOC in GaAs, which is $\gamma_{GaAs} = 16.8$ eVÅ^3 [16]. In addition, Ga and As have both atomic numbers 2× larger than those of Si and P; thus we could expect $\gamma_{Si:P}$ to be $\approx 1/16$ of the magnitude of γ_{GaAs}, rather than 18× larger, as the model indicates. In short, whilst the SOC model may look like a convincing source of the sub-band structure, the strength of the observed splitting is two orders of magnitude larger than our computed estimates.

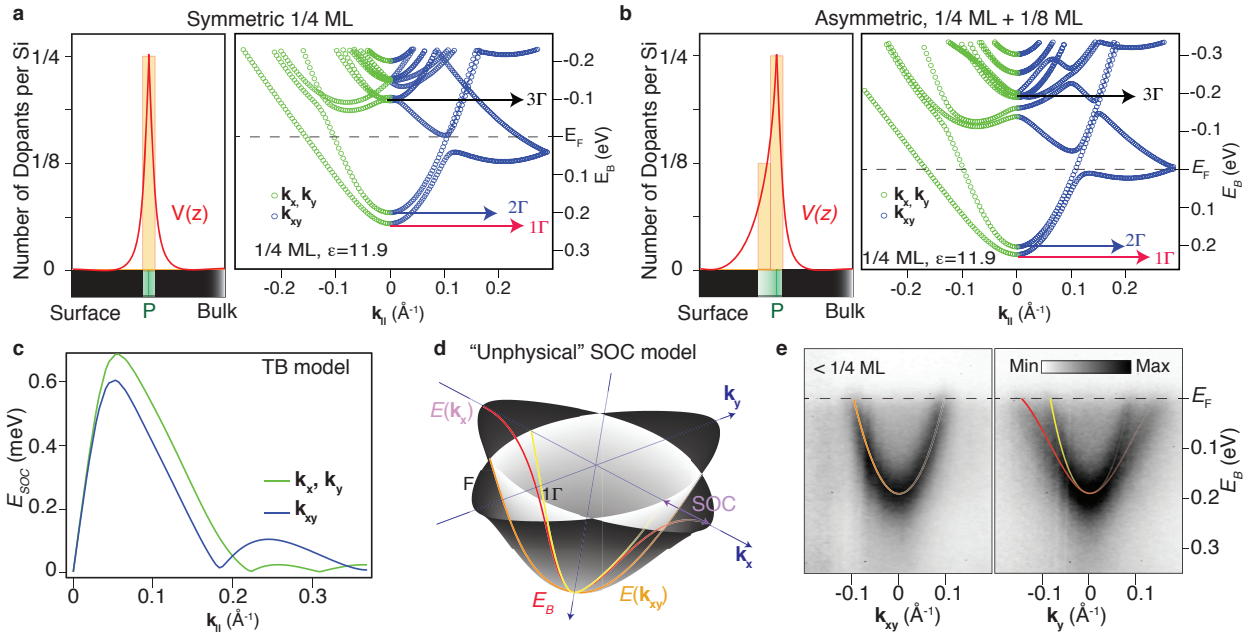

Supplementary Figure 1: An Asymmetric dopant profile, and the role of spin-orbit coupling. (a) A symmetric potential and resulting TB electronic structure, showing the well known 1Γ and 2Γ states and the unoccupied 3Γ, well above the Fermi level. (b) An asymmetric potential and the TB electronic structure showing that the main contribution of the asymmetry is to increase the 1Γ-3Γ separation ($\approx$ 400 meV) and to reduce the (1Γ-2Γ) valley-splitting. (c) Spin-orbit-coupling induced energy splitting obtained for δ-layers in silicon by relativistic tight-binding calculations. The green and blue lines correspond to the directions along which the SOC strength has been calculated, k_x ([1$\bar{1}$0]) and k_{xy} ([100]), respectively where the SOC strength has been found to be the strongest. The TB includes both Rashba, Dresselhaus and higher k-order terms. The maximum strength of the SOC is predicted to be less than 0.8 meV, a value much smaller than the energy resolution of the experiment, i.e. $\approx$ 35 meV. (d) A model for SOC from Ref. 16 has been applied to a simple parabolic dispersion in order to try to describe the states observed experimentally using ARPES. According to this model, as an effect of SOC, the band 1Γ splits into two bands, similar to the experimentally observed bandstructure. (e) Whilst the comparison of the SOC model with the experimental results is excellent, the values used to describe this spin-splitting (see main text) are physically unrealistic (i.e. $\approx$ 2 orders of magnitudes larger than indicated by TB).

EPITAXY OF SI ENCAPSULATION

Supplementary Figure 2 shows low energy electron diffraction (LEED) measurements carried out before, during and after the growth of the Si epitaxial layer. Supplementary Figure 2 shows the initial clean surface (i.e. after chemical etching and in-vacuum degassing and flashing) and indicates that a clean and well ordered 2×1 surface is formed. The pattern somewhat resembles a 2×2 reconstruction because two rotational domains are present. After PH_3 dosing and annealing to incorporate the dopants, the main structure of the LEED pattern remains unchanged (see, for example, Ref. 17). During the early stages of Si epitaxy (see Supplementary Figure 2), the 2× periodicity disappears, and a simple 1×1 pattern is seen. The pattern during growth has weaker spots and a higher background. After the growth is complete and a final anneal has been performed, a 2×1 pattern similar to the initial surface (Supplementary Figure 2(c)) reappears. We believe that the change in surface order (and the poorer quality LEED during growth) are caused by residual hydrogen from the PH_3 dissociation, which is present on the surface during Si growth, but is removed by the final annealing [17, 18].

Note: the LEED acquisitions in Supplementary Figure 2(a) and (b) have been performed using a low energy electron microscope (LEEM) with a collection area of $\approx 4\mu$m using a start voltage of 40 eV. The LEED acquisition in Supplementary Figure 2(c) used a traditional LEED unit (with spot size ≈1 mm) and with a kinetic energy of 250 eV. These two instruments are not connected, and hence the data corresponds to multiple samples and multiple preparations. In other words, the samples are comparable and prepared to a similar recipe, but not necessarily identical.

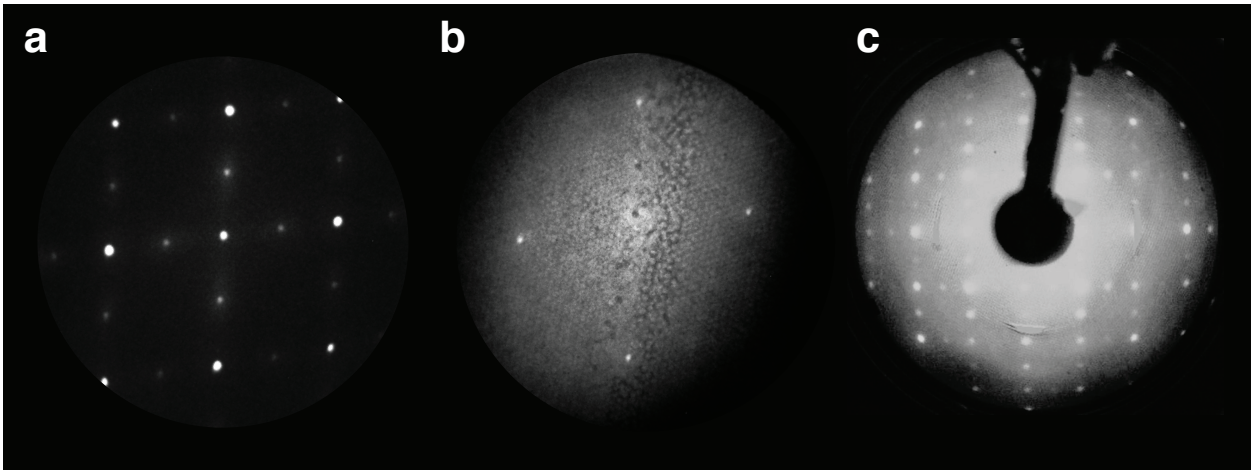

Supplementary Figure 2: The epitaxy of the Si overlayer. (a) and (b) LEED images collected using a LEEM from an initial clan surface and during the early stages of Si overgrowth, respectively. The start voltage was 40 eV and the collection area has diameter Ø $\approx 4\mu$m (c) Traditional LEED unit ($\approx$ 1 mm spot size) after the completion of the growth and after a final anneal to 500°C (in which any excess hydrogen from the PH_3 dissociation is desorbed). The kinetic energy is 250 eV.

STRAIN

One factor which can modify the electronic structure is strain. However, in this case only a small degree of strain is introduced replacing an Si atom (Z=14) with a P dopant (Z=15): For Si:P δ-layers, the strain has been estimated to be between 0.1% and 0.9% [19, 20] and the change in Si-P bond length for an isolated P dopant in an Si host is reported to be 1.7% [21]). We believe that this small degree of strain is insufficient to explain why the 3Γ states is observed to be occupied, and we have endeavoured to try to demonstrate this by performing calculations in which a realistic degree of strain is included. Specifically, we include a strain of 0.9%, i.e. corresponding to the upper limit of the existing estimates. These TB calculations are shown in Fig. S3(b), alongside an equivalent calculation in which the strain is zero. Qualitatively, the calculations look extremely similar; i.e. the effect of strain is small. On the other hand, the 1Γ-2Γ increases by a significant amount. Somewhat surprisingly, the effect on the 1Γ-3Γ separation is much less significant (i.e. 256 meV instead of 243 meV). In other words, strain does not play a large role in modifying the valley splittings, and it is unable to explain why the 3Γ state is observed to be occupied in our measurements.

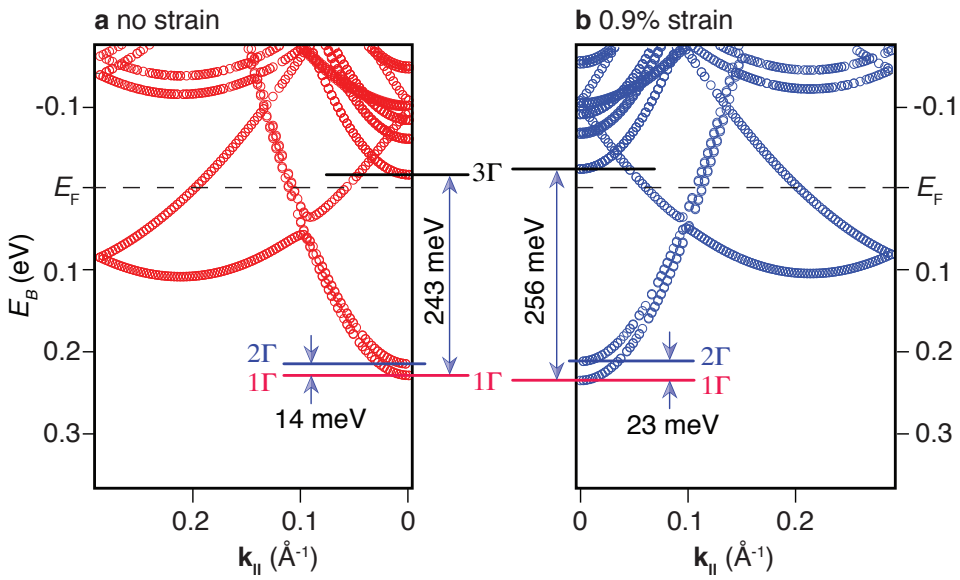

Supplementary Figure 3: The strain dependence of the valley splitting. (a) The TB calculated band structure (in the diagonal k_{xy} direction) without strain. The 1Γ-2Γ separation at the band minima is 14 meV and the 1Γ-3Γ separation is 243 meV. (b) A similar calculation performed with a realistic strain of 0.9 % (the strain has previously been estimated to be between 0.1% and 0.9% [19, 20]). When strain is included in the calculation, the 1Γ-2Γ separation becomes 23 meV and the 1Γ-3Γ separation becomes 256 meV. Whilst these changes are not negligible, strain is insufficient to account for the observed bandstructure; especially the occupation of 3Γ.

* quantum.wells@gmail.com

SUPPLEMENTARY REFERENCES

[1] J. A. Miwa, P. Hofmann, M. Simmons and J. W. Wells Direct Measurement of the Band Structure of a Buried Two-Dimensional Electron Gas. *Phys. Rev. Lett.* **110** 136801 (2013).

[2] S. R. McKibbin et al., Low resistivity, super-saturation phosphorus-in-silicon monolayer doping. *Applied Physics Letters* **104** 123502 (2014).

[3] S. Lee et al., Electronic structure of realistically extended atomistically resolved disordered Si:P δ-doped layers. *Phys. Rev. B* **84** 205309 (2011).

[4] R. Rahman et al., High Precision Quantum Control of Single Donor Spins in Silicon. *Phys. Rev. Lett.* **99** 036403 (2007).

[5] B. Weber et al., Spin blockade and exchange in Coulomb-confined silicon double quantum dots. *Nature Nanotechnology* **9** 430-435 (2014).

[6] M. Luisier, A. Schenk, A. and W. Fichtner Full-Band Atomistic Study of Source-To-Drain Tunneling in Si Nanowire Transistors. *Simulation of Semiconductor Processes and Devices* 221–224 (2007).

[7] H. Ilatikhameneh et al., Tunnel Field-Effect Transistors in 2-D Transition Metal Dichalcogenide Materials. *IEEE Journal on Exploratory Solid-State Computational Devices and Circuits* **1** 12–18 (2015).

[8] C. Chen et al., Channel Thickness Optimization for Ultrathin and 2-D Chemically Doped TFETs. *IEEE Transactions on Electron Devices* **65** 4614–4621 (2018).

[9] C. M. Polley et al., Exploring the Limits of N-Type Ultra-Shallow Junction Formation. *ACS Nano* **7** 5499-5505 (2013).

[10] Roland Winkler Spin-Orbit Coupling Effects in Two-Dimensional Electron and Hole Systems. *Springer* (2003).

[11] E. Rotenberg, J. W. Chung and S. D. Kevan Spin-orbit coupling induced surface band splitting in Li/W(110) and Li/Mo(110). *Phys. Rev. Lett.* **82** 4066-4069 (1999).

[12] R. Ferdous et al., Valley dependent anisotropic spin splitting in silicon quantum dots. *npj Quantum Information* **4** 26 (2018).

[13] R. Ferdous et al., Interface-induced spin-orbit interaction in silicon quantum dots and prospects for scalability. *Phys. Rev. B* **97** 241401 (2018).

[14] M. T. Edmonds et al., Spin–Orbit Interaction in a Two-Dimensional Hole Gas at the Surface of Hydrogenated Diamond. *Nano Letters* **15** 16–20 (2015).

[15] Y. A. Bychkov and E. I. Rashba Properties of a 2D electron gas with lifted spectral degeneracy. *Soviet Journal of Experimental and Theoretical Physics Letters* **39** 78 (1978).

[16] R. Eppenga and M. F. H. Schuurmans Effect of bulk inversion asymmetry on [001], [110], and [111] GaAs/AlAs quantum wells. *Phys. Rev. B* **37** 10923–10926 (1988).

[17] S. P. Cooil et al., In Situ Patterning of Ultrasharp Dopant Profiles in Silicon. *ACS Nano* **11** 1683–1688 (2017).

[18] H. F. wilson et al., Thermal dissociation and desorption of PH_3 on Si(001): A reinterpretation of spectroscopic data. *Phys. Rev. B* **74** 195310 (2006).

[19] D. J. Carter, O. Warschkow, N. A. Marks, and D. R. McKenzie, Electronic structure models of phosphorus δ -doped silicon *Phys. Rev. B* **79** 033204 (2009).

[20] D. W. Drumm et al., Ab initio calculation of valley splitting in monolayer δ-doped phosphorus in silicon *Nanoscale Research Letters* **8** 111 (2013).

[21] H. Overhof and U. Gerstmann Ab Initio Calculation of Hyperfine and Superhyperfine Interactions for Shallow Donors in Semiconductors *Phys. Rev. Lett.* **92** 087602 (2004).